IJE TRANSACTIONS A: Basics Vol. 32, No. 10, (October 2019) 1345-1352

International Journal of Engineering

Journal Homepage: www.ije.ir

Mesoporous WO_3/TiO_2 Nanocomposites Photocatalyst for Rapid Degradation of Methylene Blue in Aqueous Medium

L. Ernawati[a], R. A. Wahyuono*[b], A. A. Muhammad[a], A. R. Nurislam Sutanto[a], I. K. Maharsih[a], N. Widiastuti[a,c], H. Widiyandari[d]

[a] *Department of Chemical Engineering, Institut Teknologi Kalimantan, Indonesia*
[b] *Department of Engineering Physics, Institut Teknologi Sepuluh Nopember, Indonesia*
[c] *Department of Chemistry, Institut Teknologi Sepuluh Nopember, Indonesia*
[d] *Department of Physics, Universitas Sebelas Maret, Surakarta, Indonesia*

PAPER INFO

Paper history:
Received 26 July 2019
Received in revised form 04 September 2019
Accepted 12 September 2019

Keywords:
Kinetic
Nanocomposite
Photocatalyst
TiO_2
WO_3

ABSTRACT

This paper presents the wet chemical synthesis of WO_3/TiO_2 nanocomposites using hydrothermally prepared monoclinic WO_3 and anatase TiO_2 nanoparticles as composite matrices and filler, respectively. The nanocomposites were prepared in different compositions, *i.e.* WO_3:TiO_2 ratio (w/w) of (1:1), (1:3), and (3:1). Physicochemical properties of the resultant WO_3/TiO_2 nanocomposites were evaluated by X-ray diffraction (XRD), scanning electron microscopy (SEM), BET N_2 adsorption-desorption isotherms, UV/vis, and Raman spectroscopy. The resultant nanocomposites exhibited a mesoporous structure with specific surface area of up to 11.5 $m^2 g^{-1}$, where TiO_2 constituent contributed to higher surface area, especially in (1:3) ratio, and higher number of defect sites. While there was no impurities in the investigated nanocomposites as revealed by XRD analysis and Raman spectra, the WO_3:TiO_2 (1:3) nanocomposites showed the highest light harvesting ability indicated by higher absorption amplitude in both UV and visible regime. Three different kinetic models including pseudo-first-order, pseudo-second order, and Langmuir-Hinshelwood were applied to experimental data. The pseudo-second-order was found to be the best representing model and the adsorption kinetic studies indicated that chemisorption initially dominated the degradation mechanism. Finally, photocatalytic activity of nanocomposites was compared for photodegradation of methylene blue (MB) aqueous medium and in a good agreement with physicochemical properties, WO_3:TiO_2 (1:3) nanocomposites yielded the highest MB degradation rate ($k \sim 0.162$ min^{-1}) and efficiency (96%) within 120 min under UV irradiation.

***doi**: 10.5829/ije.2019.32.10a.02*

1. INTRODUCTION

A constantly increasing use of synthetic dyes in various industries, such as textiles, rubber, plastics, and food, requires discharging the colored wastewater into the environment [1-3]. Amongst various commercial synthetic dyes, methylene blue (MB) is widely utilized. Long-term exposure to MB can cause formation of Heinz bodies, and tissue necrosis in humans [3]. Therefore, removal of MB from wastewater is very important to reduce the dye hazards to the biotic environment. Currently, there are numerous methods for degradation of synthetic dyes from wastewaters, including physico-chemical and biological techniques [1-3]. However, photocatalytic degradation of MB using semiconductor catalyst has gained a great interest since its catalytic efficiency can be tuned by controlling the microstructural properties of semiconductor [4-7]. Among various n-type semiconductors, TiO_2 is widely employed due to its versatile optical properties, low cost, stability against photocorrosion, and large surface area [6, 7]. While the conduction band (CB) and valence band (VB) positions of TiO_2 are suitable to drive charge transfer for photooxidation of organic dyes, the large band gap of ~ 3.3 eV ($\lambda_{exc} \sim 375$ nm) limits its functionality which requires UV irradiation to create exciton.

*Corresponding Author Email: *ruri.tf014@gmail.com* (R. A. Wahyuono)

Please cite this article as: L. Ernawati, R. A. Wahyuono, A. A. Muhammad, A. R. Nurislam Sutanto, I. K. Maharsih, N. Widiastuti, H. Widiyandari, Mesoporous WO_3/TiO_2 Nanocomposites Photocatalyst for Rapid Degradation of Methylene Blue in Aqueous Medium, International Journal of Engineering (IJE), IJE TRANSACTIONS A: Basics Vol. 32, No. 10, (October 2019) 1345-1352

Another appealing n-type semiconductor is WO_3 which has also been extensively studied for catalysis [8]. Bearing a smaller optical band gap of ~ 2.6 eV (λ_{exc} ~ 475 nm), WO_3 enables higher light harvesting in visible regime than TiO_2 [8-10]. In spite of photocorrosion issue which leads to the formation of W^{3+} and decreases its catalytic activity, the band position is also favorable for oxidation reactions on the surface [11, 12]. Furthermore, WO_3 surface is characterized by highly negative surface charges and hence, it is advantageous for the adsorption of the cationic dye (MB). To combine the virtue of both TiO_2 and WO_3, recent studies explored WO_3/TiO_2 nanocomposites which exhibit desirable physicochemical properties for the enhanced photocatalytic activity. In addition, the nanocomposites offer other advantages [9-12]. Nanocomposites enable photocatalytic process under visible solar spectrum. The band position of WO_3 is suitable to allow excited state charge transfer to TiO_2 for efficient redox process [13,14]. Moreover, the nanocomposites reduce the synthesis cost as the price of composite material is more affordable than pure WO_3 [12]. Recent studies have reported the synthesis of WO_3/TiO_2 nanocomposites using various methods, such as sol-gel, solvothermal, hydrothermal, and alcoholthermal [10-15]. The morphology of the resulting nanocomposites also differs from unstructured porous network, spherical aggregates and hollow spheres, yielding in a unique physical to microstructural properties with promising catalytic activities [13-15]. However, it should be noted that the above mentioned method is considered time consuming and requires long synthesis routes.

In the present work, a facile and low cost approach to synthesize WO_3/TiO_2 nanocomposites by wet chemical synthesis at mild temperature is proposed. The morphology, microstructure, and optical properties of WO_3/TiO_2 nanocomposites with different compositions, *i.e.* ratio between WO_3 and TiO_2, are characterized and correlated with the photocatalytic activities for the MB degradation. Finally, the mechanism of photocatalytic degradation of MB using the nanocomposites is proposed.

2. EXPERIMENTALS

2. 1. Chemicals, Materials, and Preparation of WO_3/TiO_2 Nanocomposite The chemicals and materials, *i.e.* $Na_2WO_4.2H_2O$ (Xiqiao Chemical), CTABr (Himedia, 99%), TiO_2 (MTI, 99%), methanol (96%, UPT, BPPTK LIPI), hydrochloric acid (HCl, smart-lab), and aquadest, were used as received. Hydrothermal synthesis of WO_3 nanoparticle was carried out following the protocol developed in the literature [16] with minor modification, *i.e.* $Na_2WO_4.2H_2O$/CTABr molar ratio of 4:1 was used. The WO_3/TiO_2 nanocomposite was prepared using sol-gel method: WO_3 to TiO_2 weight ratio was set to (1:1), (1:3), and (3:1). An amount of TiO_2 was dissolved in 100 mL of aquades and sonicated for 10 min. The TiO_2 solution was then stirred (300 rpm) at 30 °C for 15 min. The powder of WO_3 nanoparticles was added into the TiO_2 solution and stirred for 15 min. The mixture solution was evaporated and dried at 80 °C for 12 h. Eventually, the dried powder was ground resulting in fine powder of WO_3/TiO_2 nanocomposite.

2. 2. Physicochemical Characterization X-ray diffraction (XRD) patterns were recorded using a PAN analytical type X'Pert Pro diffractometer with Cu-Kα as the radiation source operated at 40 kV and 40 mA. Diffraction patterns were scanned at angle (2θ) between 10 and 100° with 0.05° resolution. Crystal size was estimated by Scherrer equation. SEM images of WO_3/TiO_2 powder were measured by a scanning electron microscope (SEM, FEI type Inspect 21) operated at 100 kV accelerating voltage. BET N_2 adsorption/desorption isotherms were measured at 77 K (NOVA Touch 4LX). Prior to surface area analysis, the powdered samples were dried at 200 °C in N_2 for 3 h. Raman spectra were collected upon excitation at 785 nm (25 mW) using TEC-HR Raman Spectrometer (Stellarnet Inc) coupled with 180° degree optical probe [17]. Absorption spectra were measured using UV/vis spectrometer (Ocean optics USB4000).

2. 3. Photocatalytic Degradation of Methylene Blue Photocatalytic activity of WO_3/TiO_2 nanocomposites against organic polutant, *i.e.* methylene blue (MB), was assessed. Initial test of MB photodegradation was carried out employing WO_3 and TiO_2 nanoparticles and different WO_3/TiO_2 nanocomposites. The photocatalyst was soaked in the aqueous MB solution and then transferred into a custom-built photoreactor and irradiated under UV light for several times, *i.e.* every 15 min for 2 h. Additionally, the solution was continuously stirred to increase contact between photocatalyst and MB molecules and hence, driving a rapid photodegradation. The reactor was covered to avoid contribution from the ambient light, assuring that the photodegradation was merely driven by UV irradiation. Photodegradation of MB was detected through absorption change at 665 nm measured using UV/vis spectrometer. The decrease of MB optical density was used to determine the decreasing MB concentration due to the catalytic activity of either WO_3 nanoparticles or WO_3/TiO_2 nanocomposite.

3. RESULTS AND DISCUSSION

3. 1. Microstrutural and Optical Properties of WO_3/TiO_2 Nanocomposite Morphology of the bare

WO_3 nanoparticles and the resultant WO_3/TiO_2 nanocomposites is shown by SEM micrographs (Figure1). The morphology of WO_3 (Figure 1a) is characterized by aggregated microstructure with primary crystallites in spherical shape. The average crystallite size is estimated around 47 nm with size distribution as shown in Figure 1b. The histogram of crystallite size distribution further indicates polydispersity of WO_3. For WO_3/TiO_2 nanocomposites, the SEM image depicts the presence of WO_3 (large and aggregated particles in dark) and TiO_2 (tiny particles, white spots). Nonetheless, it can be seen that changing the ratio between WO_3 and TiO_2 alters the surface properties. Even though both nanocomposites showed agglomeration, it is also clear that WO_3/TiO_2 (1:1) nanocomposites revealed a relatively compact surface (Figure 1a) while a fractal surface characterized WO_3/TiO_2 (1:3) nanocomposite. It is worth mentioning that the nanocomposite in this work porous WO_3 was utilized as the composite matrices while smaller TiO_2 nanoparticles were used as composite filler. Hence, the very different surface morphologies can be rationalized with different hydrophilicities between TiO_2 and WO_3 within nanocomposites [18]. TiO_2 is more hydrophilic than WO_3. Increasing TiO_2 nanoparticles plausibly leads to a strong aggregation among nanoparticles which eventually breaks the structural integrity of WO_3 porous network as the matrice. As mentioned earlier, porous nanocomposite structure with larger surface area and bigger pore volume is preferred to improve the photocatalytic performance since larger specific surface areas are able to enhance the adsorption of dye molecules. BET surface area and pore structure of different nanocomposites were then investigated by the nitrogen (N_2) adsorption–desorption isotherm (Figure 2).

Barret-Joyner-Halenda (BJH) analysis for pore size distribution unravels an average pore size distribution of 4.5 and 9.5 nm for WO_3/TiO_2 (1:1) and (1:3)

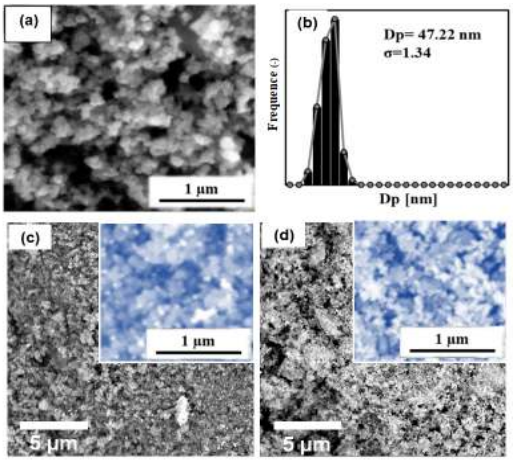

Figure 1. (a) SEM and (b) particle size distribution of WO_3. SEM image of WO_3/TiO_2 nanocomposite with different compositions (c) 1:1 and (d) 1:3

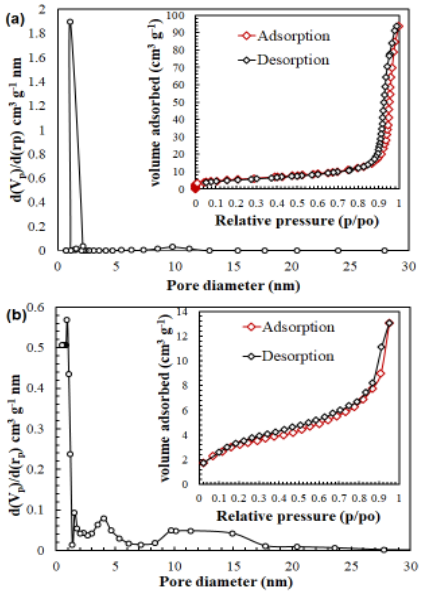

Figure 2. BJH analysis and BET N_2 adsorption-desorption curve (inset) of WO_3/TiO_2 nanocomposites with different compositions (a) 1:1 and (b) 1:3

nanocomposites, respectively, which is in agreement with SEM identification where WO_3/TiO_2 (1:3) nanocomposite shows fractal and larger porous surface. Furthermore, it reveals that both nanocomposite has mesoporous structures, i.e. pore diameters are below 50 nm. The adsorption-desorption curve is classified as Type IV isotherm curve which also indicates the presence of mesoporous structure. The presence of hysteresis loop and high adsorption at high relative pressure (p/p_0) 0.7 – 1 further indicates the presence of slit-like pores and implies the structure of large mesopores and macropores [19]. Between WO_3/TiO_2 (1:1) and (1:3) nanocomposites, isotherm of (1:3) lifted up due to the higher surface area possessed by (1:3) nanocomposites, i.e. 11.47 m^2/g vs. 4.74 m^2/g for (1:1). This indicates that TiO_2 consitutent possessed larger surface area than WO_3. Such higher specific surface area is beneficial for higher dye adsorption and eventually for photocatalytic degradation process. Nonetheless, the pore volume of both nanocomposites does not differ significantly which spans between 0.20 – 0.22 $cm^3 g^{-1}$.

A quantitative XRD analysis was carried out to unravel the underlying crystallite stucture forming the WO_3/TiO_2 nanocomposites (Figure 3). The diffraction patterns of bare WO_3 and TiO_2 utilized as nanocomposite constituents fit the monoclinic WO_3 crystal and anatase TiO_2 crystal structure according to JCPDS No. 00-043-1035 and JCPDS No. 00-021-1272, repsectively. As estimated by Debye-Scherrer formula, the crystallite size of WO_3 and TiO_2 is 46 and 75 nm, respectively. All diffraction patterns of WO_3/TiO_2 (1 :1) nanocomposite show a combination of anatase TiO_2 and WO_3 without

any impurities. Furthermore, the crystallinity of WO_3/TiO_2 nanocomposite exceeds 90%, in which the crystallite size of WO_3 (51.7 nm) and TiO_2 (73.3 nm) is not significantly altered compared with the individual crystallite size.

The purity of WO_3/TiO_2 nanocomposites was further investigated by Raman spectroscopy (Figure 4). For TiO_2, the presence of strong Raman peaks at 150 – 450 cm^{-1} indicates the metal – oxygen bonding in TiO_2. Different vibration modes in Raman spectrum of TiO_2 characterize E_g, B_g, and A_g, which are due to symmetric stretching vibration, symmetric bending vibration, and antisymmetric bending vibration of TiO_2, respectively [19]. In general, the Raman spectrum of TiO_2 corroborates the assignment of anatase TiO_2 phase in XRD analysis. Raman spectrum is altered as TiO_2 is composited with WO_3. Additional Raman bands appear at 225, 700 and 805 cm^{-1}. The band at 225 cm^{-1} is attributed to ν(W–O–W), while the bands at 700 and 805 cm^{-1} are assigned to ν(O–W–O) [10].

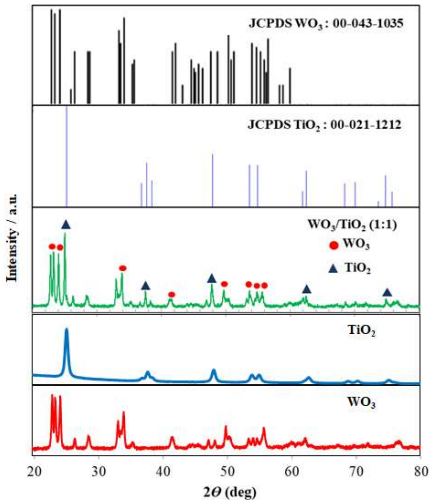

Figure 3. XRD patterns of WO_3, TiO_2, and WO_3/TiO_2 (1:1) nanocomposites

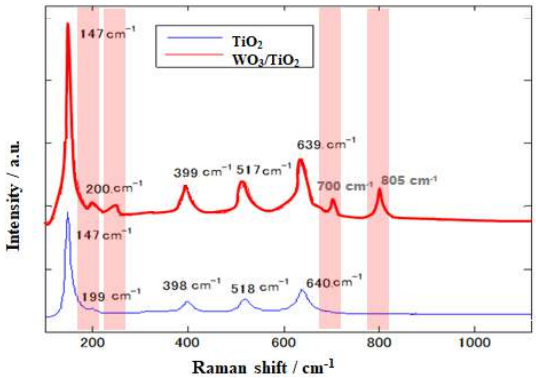

Figure 4. Raman spectra of bare TiO_2 and WO_3/TiO_2 nanocomposites upon excitation at 785 nm

UV/vis absorption spectra of WO_3/TiO_2 nanocomposites dispersed in water characterize the optical properties, particularly the light harvesting ability (Figure 5). For WO_3 constituent, it shows absorption maximum at 350 nm with a broad absorption tail in the visible region. Interestingly, the absorption spectrum of TiO_2 shows exceptionally broad and high absorption in visible region (400 – 650 nm) than UV region which is typically associated with band gap absorption. This indicates that the anatase TiO_2 used in this study possesses large concentration of defect chemistry inducing strong intraband absorption in visible regime [20]. Nonetheless, it should be noted that defect sites in metal oxide semiconductor are beneficial as these sites provide catalytic center for reduction or oxidation process. When it is composited with WO_3, in which WO_3 concentration is higher than TiO_2 (3:1), the absorption spectrum is dominated by UV absorption. Among three different compositions, WO_3/TiO_2 (1:1) nanocomposite exhibited both the strong UV-band gap absorption and broad visible absorption due to defects. Therefore, the optical properties of WO_3/TiO_2 (1:1) nanocomposite features an advantageous character for photocatalyst since it shows band gap absorption for charge separation as well as intraband absorption for catalytic center.

3. 2. Photocatalytic Degradation of MB and Kinetic Study The photocatalytic activity of mesoporous WO_3/TiO_2 nanocomposite was evaluated for the degradation of MB as organic pollutant. Initially, the absorption of MB in aqueous medium is measured as the reference absorption value for undegraded MB (10 ppm). Once the photocatalyst is added into the solution and UV irradiation is applied, the absorption intensity gradually decreases with respect to time, suggesting that the dyes are degraded in the presence of a photocatalyst under direct UV irradiation (Figure 6a). As a control experiment, photocatalytic degradation of MB using bare TiO_2 and WO_3 is also presented. Under UV irradiation, WO_3 catalyst facilitates MB degradation by 68% in 15

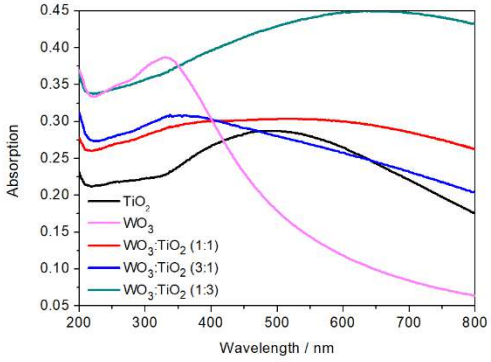

Figure 5 UV/vis absorption spectra of WO_3/TiO_2 nanocomposite with different compositions dispersed in water

min while minimum MB degradation by 42% is yielded when TiO_2 catalyst is employed. These results show the nature of MB adsorption and photocatalytic degradation in both materials. Smaller surface area in WO_3 and its negatively charge surface lead to a more rapid degradation of MB thus saturated adsorption condition is achieved fast, while adsorption of MB using TiO_2 takes longer time and hence, the degradation becomes slower. Nevertheless, the yield of MB degradation after 120 min is comparable for both, i.e. 86 and 80% for WO_3 and TiO_2, respectively.

Having characterized the performance of WO_3 and TiO_2 for MB removal, the photocatalytic degradation of MB using WO_3/TiO_2 nanocomposite is discussed. As seen, TiO_2 plays role in tuning the MB photodegradation rates. A rapid dye removal of up to 80% in merely 15 min is achieved using WO_3/TiO_2 (1:1) nanocomposite, while lower removal efficiencies of 45 and 50% are obtained for WO_3/TiO_2 (1:3) and (3:1) nanocomposite, respectively. After 60 min, WO_3/TiO_2 (1:1) nanocomposite still exhibits better efficiency of MB removal than other nanocomposites. However, after 120 min, WO_3/TiO_2 (1:3) nanocomposite yields higher MB removal efficiency of up to 92% when compared with WO_3/TiO_2 (1:3) nanocomposite resulting in a final MB removal efficiency of 89%. Therefore, it can be inferred that initial MB degradation is driven by WO_3 photocatalyst and slower reaction is facilitated by TiO_2 photocatalyst.

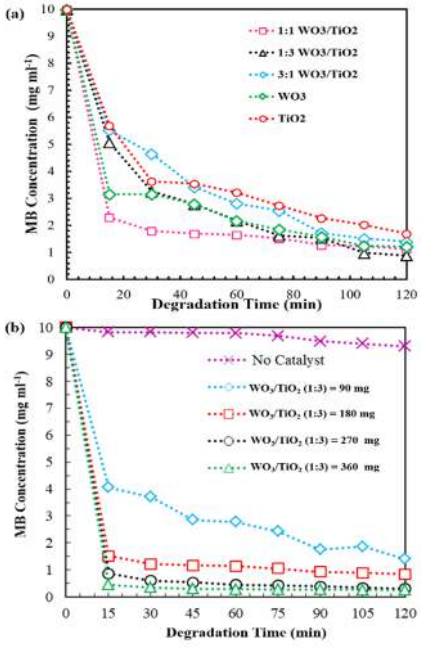

Figure 6. (a) The photocatalytic degradation profiles of MB in the presence of different catalysts under UV irradiation, (b) time dependent MB concentration in the presence of WO_3/TiO_2 (1:1) nanocomposite particle after exposure to UV irradiation under various catalyst doses

Further catalyst dose dependent study was then carried out. The results imply that increasing dose of WO_3/TiO_2 (1:3) nanocomposites from 90 to 360 mg leads to a more rapid photocatalytic MB degradation (Figure 6b). A quantitative data of temporal MB removal at different doses reveals that 80% of MB is removed using the lowest dose catalyst of 90 mg. A higher dose facilitates very rapid MB degradation within the first 15 min of irradiation, for example 96% of MB degrades in contact with 360 mg of catalyst, whilst merely 40% of MB is photodegraded using 90 mg of catalyst. A more rapid and higher MB removal at higher dose of photocatalyst is expected since the amount of adsorbed dye on catalyst as well as the light–dye–catalyst interaction increases.

To better understand the photocatalytic degradation mechanism, kinetic analysis of MB degradation using WO_3/TiO_2 nanocomposite under UV irradiation was carried out. The first kinetic model used is the pesudo-first-order model:

$$r = -\frac{dC}{dt} = k_{obs}C \quad (1)$$

By integrating the above equation, the kinetic model can be expressed as follows:

$$ln\frac{C_0}{C} = k_{obs}t \quad (2)$$

where C_o is the initial concentration in the bulk solution, t is the reaction time and k_{obs} is the observed pseudo-first-order rate constant. A plot of $ln(C_o/C_t)$ versus t will result in a linear curve, in which the slope equals to the observed rate constant of k_{obs} (Figure 7). For the pseudo-second order kinetic model, two-site-occupancy adsorption is considered. The kinetic model is represented by:

$$\frac{t}{C_t} = \frac{1}{k_2 C_e^2} + \left(\frac{1}{C_e}\right)t \quad (3)$$

The initial sorption rate is defined by the folowing equation:

$$h = k_2 C_e^2 \quad (4)$$

where C_e is dye concentration at equilibrium in solution (mg L^{-1}), C_t is the catalyst uptake capacity at any time (mmol g^{-1}), and k_2 is the pseudo-second-order rate constant (g $mmol^{-1}$ min^{-1}) which is obtained from the off-set of the linear plot of t/C_e vs t. Kinetic rate constants determined from both kinetic models are summarized in Table 1.

In addition, other kinetic model, i.e. Langmuir-Hinshelwood (L-H), is applied to the data for comparison:

$$\frac{C_e}{q_e} = \frac{1}{K_L q_m} + \frac{C_e}{q_m} \quad (5)$$

where q_m is the Langmuir constant related to adsorption capacity (mg g^{-1}), K_L is the adsorption rate (mg L^{-1}), q_e is the dye concentration at equilibrium on WO_3/TiO_2

nanocomposite (mg L^{-1}), and C_e is dye concentration at equilibrium in solution (mg L^{-1}) (see Table 2).

Kinetic of photocatalytic degradation of MB using WO_3/TiO_2 nanocomposite is discussed as follows: The variation of catalyst concentration as a function of irradiation time gives a linear fit curve (Figure 7). The results clearly denote that the photocatalytic reaction on WO_3/TiO_2 nanocomposite is found best to follow the pseudo-second-order kinetic than the pseudo-first-order kinetic model. This indicates that the molecules are mainly chemisorbed rather than physisorbed onto the catalyst surface before photocatalytic degradation occurs. In addition, L-H kinetic model fails to represent the degradation mechanism indicated by lower R^2, and hence, two molecules adsorbtion at neighboring sites are not the main mechanism on the investigated system here. According to the pseudo-second-order kinetic model the value of k (0.162 min^{-1}) is found to be highest for the MB degradation corresponding to the utilization of WO_3/TiO_2 (1:1) nanocomposite. Compared with other studies, the resulting rate constant for bare anatase TiO_2 (k ~ 0.024 min^{-1}) is comparable and slightly better than that of C-doped TiO_2 (k ~ 0.01 min^{-1}) under UV irradiation [21]. The use of mesoporous WO_3 prepared here also outperforms the photocatalytic degradation rate of MB using other mesoporous WO_3 prepared from amonium metatungstate [22], *i.e.* 0.041 *vs.* 0.0025 min^{-1}. Comparing the degration rate of MB with WO_3/TiO_2 hollow spheres [23], *i.e.* 0.162 vs 0.041 min^{-1}, the present work already exhibits promising materials for photocatalysis.

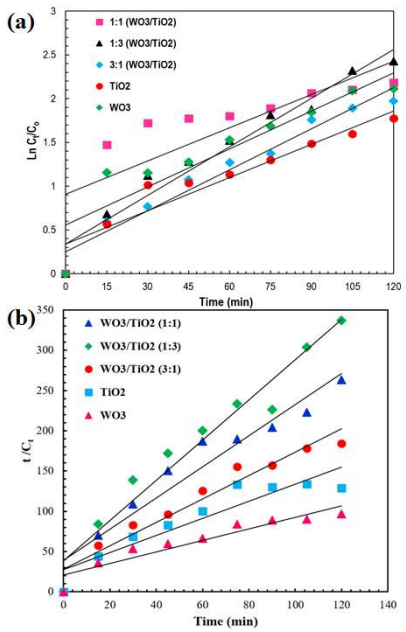

Figure 7. (a) Pseudo-first-order and (b) pseudo-second-order kinetics plots of MB degradation under UV irradiation in the presence of various photocatalysts

TABLE 1. Rate constant of MB degradation derived from pseudo first-order and second-order kinetic models

Photocatalyst	k_{obs} (min^{-1})	R^2	k_2 (min^{-1})	R^2
WO_3/TiO_2 (1:1)	0.0127	0.72	0.162	0.95
WO_3/TiO_2 (1:3)	0.0185	0.96	0.096	0.93
WO_3/TiO_2 (3:1)	0.0156	0.95	0.075	0.94
WO_3	0.0145	0.85	0.041	0.86
TiO_2	0.0117	0.90	0.024	0.89

TABLE 2. Langmuir-Hinshelwood constant and correlation coefficient for the degradation of MB using WO_3/TiO_2 composite photocatalyst.

WO_3/TiO_2 Compositions	K_L (mg L^{-1})	q_m (mg g^{-1})	R^2
(1:1)	0.691	13.49	0.857
(1:3)	0.741	18.28	0.727

3. 3. Photocatalytic Degradation Mechanism of Methylene Blue The photocatalytic degradation mechanism of MB adsorbed onto WO_3/TiO_2 nanocomposite surface involves sequential charge separation and charge transfers (Figure 8). Initial charge separation occurs in WO_3/TiO_2 composite upon UV irradiation. As UV irradiation (λ ~ 365 nm, E ~ 3.4 eV) is applied and is higher than the optical band gap of WO_3 (2.7 eV) and TiO_2 (3.2 eV), the absorbed photons creates exciton in both WO_3 and TiO_2, that is a charge separated state between photoexcited electron in the conduction band (CB) and hole in the valence band (VB).

Once charge separated state is formed, the possible charge transfers between WO_3 and TiO_2 are as follows: the excited electron is transferred from the CB of TiO_2 to the CB of WO_3, while the hole in VB of WO_3 is injected to the VB of TiO_2. These charge transfer likely occur due to the more positive VB and CB position of TiO_2 than

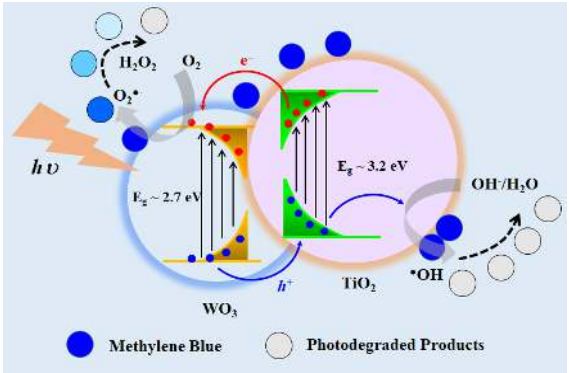

Figure 8. Proposed photocatalytic degradation mechanism of MB by WO_3/TiO_2 nanocomposite under UV irradiation

WO_3 and hence, the Gibbs free energy (ΔG) indicating the strength of driving force for electron and hole transfer is exergonic (thermodynamically possible). The photoexcited and accumulated electrons and holes eventually react with H_2O_2 and H_2O, respectively, to form OH• radicals (Equations (7)– (9)). However, these charge transfer are not always necessary since the band energy level of both WO_3 and TiO_2 already allows for inducing redox reaction with H_2O_2 and H_2O forming OH• radicals and both are capable of photocatalytically degrading the chemisorbed MB on either WO_3 or TiO_2 part under UV irradiation.

$$WO_3/TiO_2 + hv \rightarrow e^-_{CB} + h^+_{VB} \quad (6)$$

$$h^+ + H_2O \rightarrow H^+ + OH^- \quad (7)$$

$$h^+ + OH^- \rightarrow OH\bullet \quad (8)$$

$$e^- + H_2O_2 \rightarrow OH\bullet + OH^- \quad (9)$$

These OH• radicals formation are essential to oxidize and reduce the adsorbed MB molecules yielding the carbon dioxide, H_2O, and other photodegraded molecules. It should be noted that there is a driving force in the surface of photocatalyst enabling the desorption of photodegraded products from the active site to the bulk. This mechanism corresponds to the regeneration of active site in WO_3/TiO_2 associated with the photocatalytic cycle. Furthermore, the reaction between electrons and holes with H_2O_2 and H_2O, respectively, competes with the recombination reaction, which is undesirable as the produced heat considerably reduces the photocatalytic activity.

4. CONCLUSION

Photocatalyst of WO_3/TiO_2 nanocomposites were successfully prepared by wet chemical synthesis. The investigated WO_3/TiO_2 nanocomposites showed highly mesoporous structure and the WO_3:TiO_2 ratio was varied, *i.e.* (1:1), (1:3), and (3:1) in them. Physical characterization indicated that the higher TiO_2 content in nanocomposites not only contributed to larger surface area but also to more defects site as indicated by intraband visible absorption. WO_3:TiO_2 (1:3) nanocomposite showed the highest degradation rate and MB degradation efficiency (89%) within 120 min. WO_3 constituent played role in the initial adsorption and rapid degradation, whilst TiO_2 nanoparticles were essential to enlarge the adsorption sites and were responsible for slow degradation mechanism. The pseudo-second-order model best fitted the removal of MB in aqueous solution indicating that chemisorption is the initial adsorbtion mechanism followed by photocatalytic processes. Future study on the improvement of catalytic efficiency of WO_3/TiO_2 photocatalyst and organic dye degradation rate under UV/vis irradiation should be considered for further practical application.

5. REFERENCES

1. Holkar, C. R., Jadhav, A. J., Pinjari, D. V., Mahamuni, N. M., Pandit, A. B., "A critical review on textile wastewater treatments: possible approaches", ***Journal Environmental Managements***, Vol. 182, (2016), 351-366.
2. Chong, M. N., Jin, B, Chow, C. W, Saint, C., "Recent developments in photocatalytic water treatment technology: A review", ***Water Res***., Vol. 44, (2010), 2997–3027.
3. Bhima, A. N., Park, J.-H., Cho, M., Yi, Y.-J., Oh, S.-G., Park, Y.-J., Lovanh, N., Kamala-Kannan, S., Oh, B.-T., "Simultaneous utilization of soju industrial waste for silica production and its residue ash as effective cationic dye adsorbent", ***e-Polymers***, Vol. 15, No. 6, (2015), 427-437.
4. Keyvanloo, T., Asadian, K., "Effect of Formation of Ag2Ti4O9 Phase on Photocatalytic Activity of Ag-TiO2 Nanocomposite", ***International Journal of Engineering, Transaction B: Applications***, Vol. 29, No. 5, (2016), 663-668.
5. Hosseingholi, M., Hosseinnia, A., Pazouki, M., "Room Temperature Synthesis of N-doped Urchin-like Rutile TiO2 Nanostructure with Enhanced Photocatalytic Activity Under Sunlight", ***International Journal of Engineering, Transaction B: Applications***, Vol. 28, No. 10, (2015), 1401-1407.
6. Kordhaghi, F., Sadrnezhaad, S. K., "Synthesis and Characterization of Anatase-coated Multiwall Carbon Nanotube for Improvement of Photocatalytic Activity", ***International Journal of Engineering, Transaction B: Applications***, Vol. 30, No. 4, (2017), 543-550.
7. Li, Y. F., Zhang, W. P., Li, X., Yu, Y., "TiO2 nanoparticles with high ability for selective adsorption and photodegradation of textile dyes under visible light by feasible preparation", ***Journal of Physics and Chemistry of Solids***, Vol. 5, (2014), 86-93.
8. Hosseinpour-Mashkani, S. M., Maddahfar, M., Sobhani Nasab, A., "Precipitation, synthesis, characterization, morphological control and photocatalyst application of $ZnWO_4$ nanoparticles", ***Journal of Electronic Materials***, Vol. 45, No. 7, (2016), 3612-3620.
9. Hunge, Y. M., Yadav, A. A., Mahadik, M. A., Bulakhe, R. N., Shin, J. J., Mathe, V. L., Bhosale, C. H., "Degraation of organic dyes using spray deposited nanocrystalline stratified WO_3/TiO_2 photoelectrodes under sunlight illumination", ***Optical Material***, Vol. 76, (2018), 260-270.
10. Hunge, Y. M., Mahadik, M. A., Moholkar, A. V., Bhosale, C. H., "Photoelectrocatalytic degradation of oxalic acid using WO_3 and stratified WO_3/TiO_2 photocatalysts under sunlight illumination", ***Ultrasonic Sonochemistry,*** Vol. 35, (2017), 233-242.
11. Patio, S. M., Deshmukh, S. P., More, K. H., Shevale, V. B., Mullani, S. B., Dhodamani, A. G., Delekar, S. D., "Sulfated TiO_2/WO_3 nanocomposite: An Efficient photocatalyst for degradation of Congo red and methyl red dyes under visible light irradiation", ***Journal Materials Chemistry and Physics***, Vol. 225, (2019), 247-255.
12. P. Panda, C. Gopinathan. "Synthesis and Characterization of TiO_2-NiO and TiO_2-WO_3 nanocomposites", ***Journal of Materials Science: Materials in Electronics,*** Vol. 28, No. 7, (2017), 5222-5234.
13. Wang, F., Chen, X., Hu, X., Wong, K. S., Yu, J. C., "WO_3/TiO_2 microstructures for enhanced photocatalytic oxidation", ***Separation and Purification Technology***, Vol. 91, (2012), 67-72.
14. Sun, D., Liu, J., Li, J., Feng, Z., He, L., Zhao, B., Wang, T., Li., R., Yin, S., Sato, T., "Solvothermal synthesis of spindle-like WO_3-TiO_2 particles with enhanced photocatalytic activity", ***Material Research Bulletin***, Vol. 53, No. 1, (2014), 163-168.

15. Li, Y., Chen, L., Guo, Y., Sun, X., Wie, Y., "Preparation and characterization of WO_3/TiO_2 hollow microsphere composite with catalytic activity in dark", ***Chemical Engineering Journal***, Vol. 181-182, No. 2, (2012), 734-739.
16. Petsom, K., Kopwitthaya, A., Horphathum, M., Ruangtaweep, Y., Sangwarantee, N., Kaewkhao, J., "Shape-controlled synthesis of tungsten oxide nanostructures and characterization", ***Journal of Metals, Materials and Minerals***, Vol. 28, (2018), 69-75.
17. Roekmono, Hadi, H., Imtihani, H. N., Muhimmah, L. C., Yuwono, R. A., Wahyuono, R. A., "Glucose and Cholesterol Sensing in Blood Plasma Using ZnO-paper based Microfluidics", ***International Journal of Drug Delivery Technology***, Vol. 8, No. 4, (2018),
18. Wang, X., Wei, Z., Yu, C., Zhang, X., Zhang, Y., "Reversible Wettability of Tungsten Trioxide Films with Novel Dandelion-like Structures"*,**Zeitschrift für Anorganische und Allgemeine Chemie*** Vol. 638, No. 1, (2012), 231–235.
19. Wahyuono, R. A., Risanti, D. D., "Quasi-solid State DSSC Performance Enhancement by Bilayer Mesoporous TiO_2 Structure Modification", ***Advanced Materials Research***, Vol. 789, (2013), 93-96.
20. Wahyuono, R. A., Hermann-Westendorf, F., Dellith, A., Schmidt, C., Dellith, J., Plentz, J., Schulz, M., Presselt, M., Seyring, M., Rettenmeyer, M., Dietzek, B., "Effect of annealing on the sub-bandgap, defects and trapping states of ZnO nanostructures", ***Chemical Physics***, Vol. 483, (2017), 112-121.
21. Shao, X., Lu, W., Zhang, R., Pan, F., "Enhanced photocatalytic activity of TiO_2-C hybrid aerogels for methylene blue degradation"., ***Scientific Reports,*** Vol. 3, No.1, (2013), 3018-3021.
22. DePuccio, D. P., Botella, P., Rourke, B. O., Landry, C. C., "Degradation of methylene blue using porous WO_3, SiO_2-WO_3, and their Au-loaded analogs: Adsorption and photocatalytic studies", ***ACS Applied Materials & Interfaces***, Vol. 7, No. 3, (2015), 1987-1996.
23. Lv, K., Li, J., Wing, X., Li, W., Chen, Q., "Synthesis and photo-degradation application of WO_3/TiO_2 hollow spheres", ***Journal of Hazardous Materials.***, Vol. 189, No. 2, (2011), 329-335.

Mesoporous WO_3/TiO_2 Nanocomposites Photocatalyst for Rapid Degradation of Methylene Blue in Aqueous Medium

L. Ernawati[a], R. A. Wahyuono[b], A. A. Muhammad[a], A. R. Nurislam Sutanto[a], I. K. Maharsih[a], N. Widiastuti[a,c], H. Widiyandari[d]

[a] *Department of Chemical Engineering, Institut Teknologi Kalimantan, Indonesia*
[b] *Department of Engineering Physics, Institut Teknologi Sepuluh Nopember, Indonesia*
[c] *Department of Chemistry, Institut Teknologi Sepuluh Nopember, Indonesia*
[d] *Department of Physics, Universitas Sebelas Maret, Surakarta, Indonesia*

P A P E R I N F O

Paper history:
Received 26 July 2019
Received in revised form 04 September 2019
Accepted 12 September 2019

Keywords:
Kinetic
Nanocomposite
Photocatalyst
TiO_2
WO_3

چکیده

در این مطالعه سنتز شیمیائی نانوکامپوزیت WO_3/TiO_2 با روش هیدروترمال از WO_3 و نانوذرات TiO_2 **که** به ترتیب به عنوان ماتریکس کامپوزیت و فیلر مورد استفاده قرار گرفتند ارائه می‌شود. نانوکامپوزیت‌ها با ترکیبهای مختلف ۱:۱، ۱:۳ و ۳:۱ از WO_3:TiO_2 تهیه شدند. بررسی خواص فیزیکوشیمیائی نانوکامپوزیت‌ها با آنالیزهای XRD، SEM، BET، UV-vis و رامان انجام شد. نانوکامپوزیت‌های سنتز شده ساختار مزوحفره با سطح ویژه ۱۱/۵ مترمربع به گرم داشتند در حالی که TiO_2 موجب افزایش سطح ویژه و تعداد بیشتر جایگاههای فعال شد. طبق آنالیز XRD و رامان، نانوکامپوزیت‌ها ناخالصی نداشتند و نانوکامپوزیت با نسبت ۱:۳ WO_3:TiO_2 بیشترین قدرت جذب نور را در محدوده ی نور مرئی و ماورابنفش داشت. سه مدل سینتیکی شبه درجه یک، شبه درجه دو و لانگمایر–هنشل وود برای تفسیر داده‌های آزمایشگاهی استفاده شد. بر اساس مطالعات سینتیکی بهترین فیت از مدل شبه درجه دو حاصل شد که نشان دهنده این بود که مکانیزم تجزیه عمدتا تابع جذب شیمیائی است. در نهایت، فعالیت فتوکاتالیستی نانوکامپوزیت‌ها برای تجزیه متیلن بلو بررسی شد؛ نانوکامپوزیت با نسبت ۱:۳ WO_3:TiO_2 بیشترین سرعت تجزیه متیلن بلو (۰/۱۶۲ بر دقیقه) و بازدهی (۹۶٪) را در مدت ۱۲۰ دقیقه تحت تابش ماورابنفش داشت.

***doi**: 10.5829/ije.2019.32.10a.02*